iScience

CellPress
OPEN ACCESS

Article

Ibrutinib-induced pulmonary angiotensin-converting enzyme activation promotes atrial fibrillation in rats

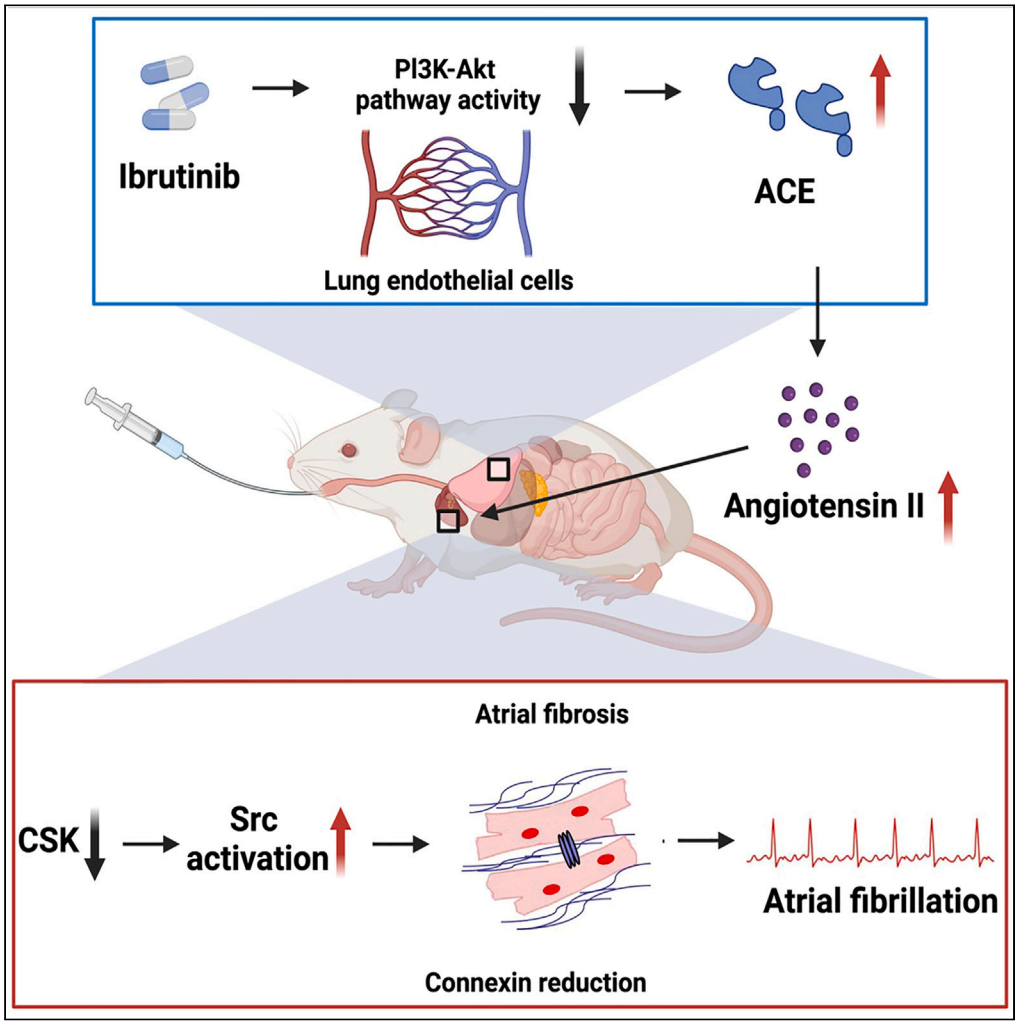

Sen Yan, Wei Xu, Ning Fang, ..., Song Zhang, Yongtai Gong, Yue Li

gongth@126.com (Y.G.)
ly99ly@vip.163.com (Y.L.)

Highlights

Ibrutinib promotes left atrial remodeling via the CSK-Src signaling pathway

Ibrutinib elevates circulating ACE and Ang II levels

Inhibition of PI3K-AKT as potential mechanism for ACE upregulation

Perindopril reverses the increased AF susceptibility caused by Ibrutinib

Yan et al., iScience 27, 108926
February 16, 2024
https://doi.org/10.1016/j.isci.2024.108926

iScience

CellPress
OPEN ACCESS

Article

Ibrutinib-induced pulmonary angiotensin-converting enzyme activation promotes atrial fibrillation in rats

Sen Yan,[1,7] Wei Xu,[1,7] Ning Fang,[1,7] Luyifei Li,[1] Ning Yang,[1] Xinbo Zhao,[1] Hongting Hao,[1] Yun Zhang,[1] Qian Liang,[1] Zhiqi Wang,[1] Yu Duan,[1] Song Zhang,[1] Yongtai Gong,[1,*] and Yue Li[1,2,3,4,5,6,8,*]

SUMMARY

The molecular mechanism of ibrutinib-induced atrial fibrillation (AF) remains unclear. We here demonstrate that treating rats with ibrutinib for 4 weeks resulted in the development of inducible AF, left atrial enlargement, atrial fibrosis, and downregulation of connexin expression, which were associated with C-terminal Src kinase (CSK) inhibition and Src activation. Ibrutinib upregulated angiotensin-converting enzyme (ACE) protein expression in human pulmonary microvascular endothelial cells (HPMECs) by inhibiting the PI3K-AKT pathway, subsequently increasing circulating angiotensin II (Ang II) levels. However, the expression of ACE and Ang II in the left atria was not affected. Importantly, we observed that perindopril significantly mitigated ibrutinib-induced left atrial remodeling and AF promotion by inhibiting the activation of the ACE and its downstream CSK-Src signaling pathway. These findings indicate that the Ibrutinib-induced activation of the ACE contributes to AF development and could serve as a novel target for potential prevention strategies.

INTRODUCTION

Ibrutinib, a novel and highly effective inhibitor of Bruton tyrosine kinase, has received approval for the treatment of chronic lymphocytic leukemia, mantle cell lymphoma, Waldenstrom macroglobulinemia, and marginal cell lymphoma.[1] However, an alarming rise in the occurrence of AF has been observed in patients undergoing ibrutinib treatment.[2,3] The initial randomized controlled trials reported a new-onset AF incidence of approximately 4%–6%.[3] Long-term studies indicate that AF develops in up to 16% of patients receiving ibrutinib over a median follow-up period of 28 months.[4] AF often leads to the discontinuation or dose reduction of ibrutinib[5] and it can also elevate the risk of thromboembolic stroke and heart failure, contributing to substantial morbidity and mortality.[6] Managing ibrutinib-induced AF presents challenges due to the delicate balance required between the benefits of anticoagulation and the increased bleeding risk associated with ibrutinib therapy.[7,8]

Despite its clinical significance, the precise mechanisms underlying ibrutinib-induced AF remain unclear. McMullen et al. proposed that the inhibition of cardioprotective PI3K-Akt signaling may be a potential mechanism for AF development in patients treated with ibrutinib.[9] Using a mouse model of 4-week ibrutinib administration, Jiang et al. reported that AF induction could be attributed to atrial structural remodeling and calcium handling disorders.[10] Yang et al. suggested that the increased signaling of reactive oxygen species in cardiomyocytes contributes to ibrutinib-induced AF.[11] More recently, Xiao et al. made a significant breakthrough by demonstrating that the elevated incidence of AF with ibrutinib is associated with its off-target inhibitory effect on CSK.[12] This finding provides valuable insights into the pathophysiology of ibrutinib-induced AF.

CSK functions as an inhibitor of Src, and its inhibition can lead to Src activation.[13] Interestingly, previous studies have demonstrated the significant involvement of Src in Ang II signaling.[14] Activation of the renin-angiotensin system (RAS) has been implicated in the initiation and perpetuation of AF through atrial remodeling.[15] These findings prompt the question of whether RAS activation, via the CSK-Src pathway, contributes to ibrutinib-induced AF. Notably, inhibitors of the RAS, such as ACE inhibitors and Ang II receptor blockers, have shown efficacy in preventing AF.[16] Hence, we hypothesized that if RAS activation is indeed involved in ibrutinib-induced AF, RAS inhibitors may confer beneficial effects.

[1]Department of Cardiology, the First Affiliated Hospital, Harbin Medical University, Harbin 150001, China
[2]NHC Key Laboratory of Cell Transplantation, Harbin Medical University, Heilongjiang 150001, China
[3]Key Laboratory of Hepatosplenic Surgery, Harbin Medical University, Ministry of Education, Harbin 150001, China
[4]Key Laboratory of Cardiac Diseases and Heart Failure, Harbin Medical University, Harbin 150001, China
[5]Heilongjiang Key Laboratory for Metabolic Disorder & Cancer Related Cardiovascular Diseases, Harbin 150081, China
[6]Institute of Metabolic Disease, Heilongjiang Academy of Medical Science, Harbin, China
[7]These authors contributed equally
[8]Lead contact
*Correspondence: gongth@126.com (Y.G.), ly99ly@vip.163.com (Y.L.)
https://doi.org/10.1016/j.isci.2024.108926

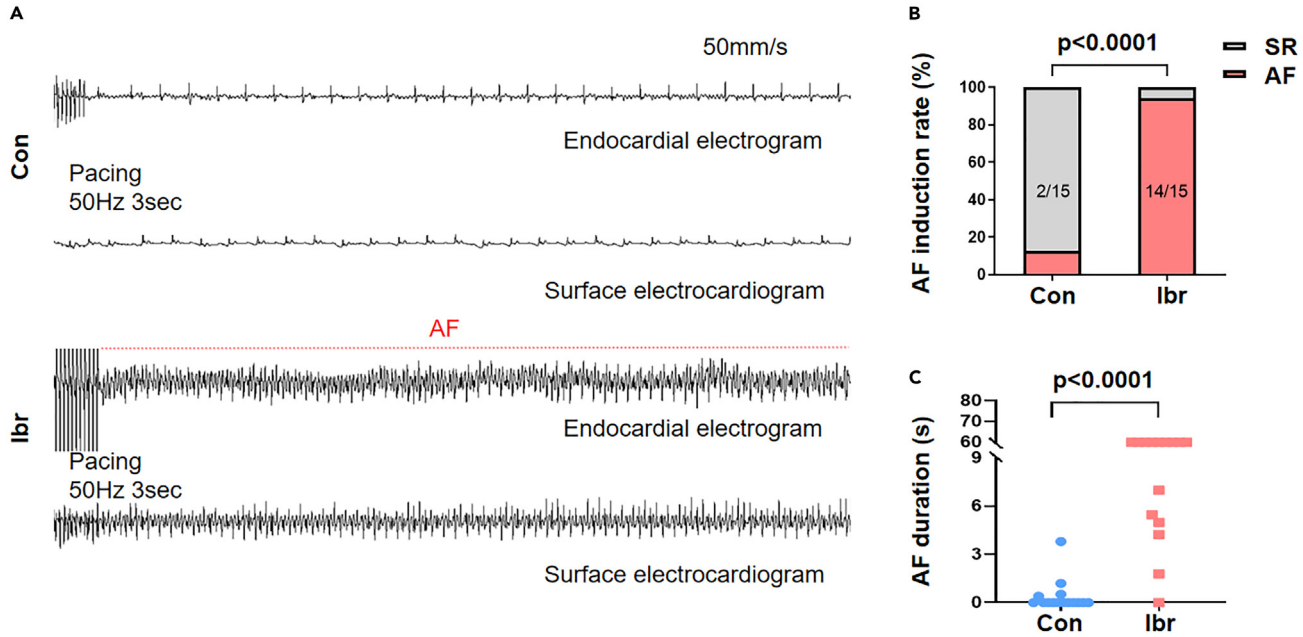

Figure 1. Ibrutinib increased AF susceptibility

(A) Representative examples of AF induction attempts in a control group rat and in an ibrutinib group rat.

(B) AF inducibility.

(C) AF duration. AF inducibility (B) was presented as numbers and compared by using the Fisher exact test. Data (C) are expressed as mean ± SEM and compared by Wilcoxon test. Con = control group; Ibr = ibrutinib group; AF = atrial fibrillation; SR = sinus rhythm; n = 15 per group.

The objective of this study was to explore the impact of ACE expression modulation in the context of ibrutinib-induced AF in rats with pre-existing AF risk factors, while also investigating the potential preventive effects of ACE inhibitors.

RESULTS

Ibrutinib increased atrial fibrillation susceptibility

As depicted in Figure 1A, atrial burst pacing rarely induced AF in control rats, while it frequently induced AF in rats from the ibrutinib group. The inducibility of AF was significantly higher in the ibrutinib group, with 14 out of 15 rats (93.3%) showing inducibility, compared to only 2 out of 15 control rats (13.3%; Figure 1B). Furthermore, AF duration was markedly prolonged in the ibrutinib group (37.57 ± 7.35 s) compared to the control group (0.40 ± 0.26 s; Figure 1C). These findings suggest that ibrutinib increases susceptibility to AF. However, no significant differences were observed between the two groups in terms of atrial effective refractory period (AERP, Figure S1A) and ion channel protein expression (Figures S1B and S1C). To address the potential influence of blood pressure reduction on atrial remodeling and AF inducibility, we conducted additional experiments using amlodipine besylate as an antihypertensive control treatment in Ibrutinib-induced AF. In comparison to the Ibrutinib group, the Ibrutinib+amlodipine besylate group effectively lowered blood pressure in the rats (Figure S2A). However, it did not reduce the AF induction rate and AF duration (Figures S2B and S2C).

Impact of ibrutinib on left atrial remodeling in rats through the modulation of the C-terminal Src kinase -Src signaling pathway

To gain insight into the mechanisms underlying the promotion of AF by ibrutinib, we investigated left atrial structural changes. Echocardiography analysis revealed a significant increase in LA diameter (Figures 2A and 2B) in the ibrutinib group compared to the control group. However, no significant change was observed in LVEF (Figure 2C) or various other parameters, including IVSD, iIVSS, LVIDD, LVIDS, LVPWD, and LVPWS (Figure S3A). Systolic and diastolic blood pressure showed a trend of increase at 2-, 3-, and 4-week intervals in the ibrutinib group rats compared to the control group rats, although the observed changes did not reach statistical significance (Figure 2D).

Hematoxylin and eosin (HE) staining of the left atrial tissues revealed well-organized fibers in the control group, characterized by a lack of intercellular spaces, whereas the ibrutinib-treated group displayed disordered myocardial fibers with hypertrophic and edematous cardiomyocytes (Figure S3B). Masson's trichrome staining demonstrated significantly increased left atrial collagen deposition and a higher collagen volume fraction in the left atrial of the ibrutinib group rats compared to the control group rats (Figure 2E). Furthermore, western blot analysis of left atrial tissues showed significant upregulation of fibrosis-related proteins, including collagen I, collagen III, transforming growth factor β

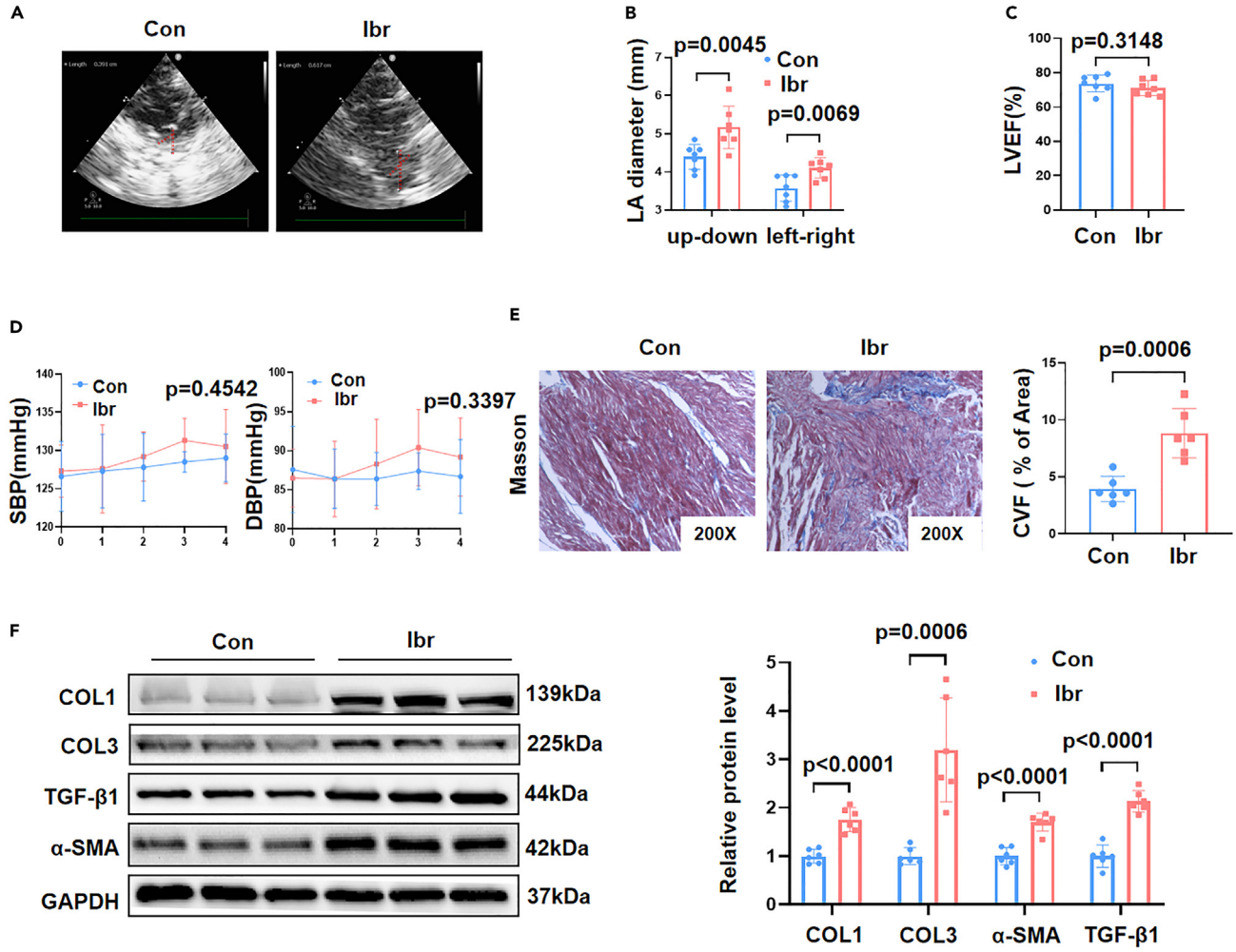

Figure 2. Ibrutinib-induced left atrial remodeling

(A) Representative echocardiography images of LA dimensions in the control and ibrutinib groups.

(B) LA diameter in the two groups (n = 7 per group).

(C) LVEF in the two groups (n = 7 per group).

(D) SBP and DBP in the two groups (n = 10 per group).

(E) Representative Masson's trichrome staining of atrial tissue and CVF of each group (n = 6 per group).

(F) Representative Western blots and quantification of protein expressions of Col I, Col III, α-SMA, and TGF-β1 in left atrial tissue of control and ibrutinib groups (n = 6 per group). Data are represented as mean ± SEM and compared by Student's *t* test. LA = left atrial; LVEF = left ventricular ejection fraction; SBP = systolic blood pressure; DBP = diastolic blood pressure; CVF = collagen volume fraction; Col I = collagen I; Col III = collagen III; Con = control group; Ibr = ibrutinib group.

1 (TGF-β1), and alpha-smooth muscle actin (α-SMA), in the ibrutinib group compared to the control group (Figure 2F). These results provide evidence that ibrutinib can induce left atrial interstitial fibrosis and left atrial enlargement.

A recent study demonstrated the inhibition of CSK contributed to ibrutinib-induced left atrial enlargement and atrial fibrosis in mice.[12] CSK functions as an inhibitor of Src, and its inhibition leads to the activation of Src, which has been shown to play a crucial role in Ang II-induced fibrosis-related changes by regulating downstream molecules such as α-SMA and TGF-β1 in cardiac fibroblasts.[17] However, the involvement of Src activation in ibrutinib-induced AF remains unclear. Thus, we examined the protein expression of CSK and Src in atrial tissues from both groups. The results revealed that ibrutinib significantly decreased CSK expression and increased Src phosphorylation (Figures 3A and 3B). Furthermore, Src activation may lead to a reduction in cardiac connexin 43 (Cx43) expression induced by Ang II.[18] Therefore, we investigated the protein expression of Cx43 in the atrial tissue of both groups and observed a significant decrease in Cx43 levels in the ibrutinib group compared to the control group (Figures 3C and 3D). Additionally, the expression of another gap junction protein, cardiac connexin 40 (Cx40), was also lower in the ibrutinib group compared to the control group (Figures 3C and 3D). These findings suggest that ibrutinib-induced atrial remodeling may be mediated through the CSK-Src signaling pathway.

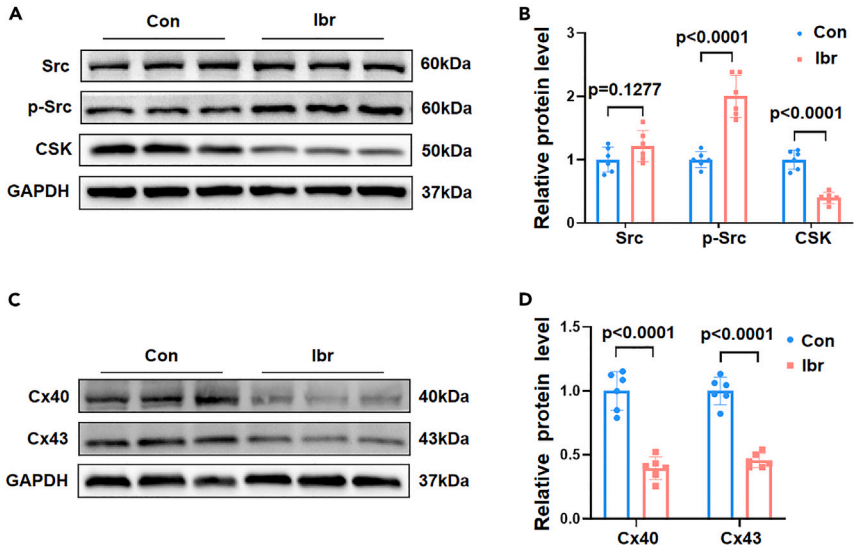

Figure 3. The protein expression of CSK, Src, CX40 and CX43 in left atrial tissue

(A and B) Representative Western blots and quantification of protein expressions of Src, *p*-Src, and CSK in left atrial tissue of control and ibrutinib groups. (C and D) Protein expressions of CX40 and CX43 in left atrial tissue of the two groups. Data are represented as mean ± SEM and compared by Student's *t* test. *p*-Src = phosphorylated Src; Cx40 = connexin 40; Cx43 = connexin 43; Con = control group; Ibr = ibrutinib group; n = 6 per group.

Ibrutinib elevates circulating angiotensin-converting enzyme and angiotensin II levels

As mentioned earlier, previous studies have demonstrated that Src activation is an early event in the signal transduction induced by Ang II.[14,18] Therefore, we hypothesized whether ibrutinib could induce the activation of the RAS. To investigate this, we measured the levels of ACE and Ang II in plasma and atrial tissues of both groups. Additionally, we assessed the plasma levels of REN, AGT, ALD, and renin activity in both groups. Surprisingly, there was no significant difference in plasma REN content and renin activity between the two groups (Figures 4A and 4B). The results showed a significant increase in plasma ACE and Ang II levels in the ibrutinib group compared to the control group (Figures 4C and 4D). However, no significant difference was observed in ACE mRNA expression and Ang II concentration in atrial tissues between the two groups (Figures 4E and 4F). Similarly, there was no significant difference in AGT and ALD between the two groups in plasma (Figures 4G and 4H). It is worth noting that serum ACE is primarily derived from vascular endothelial cells, particularly pulmonary microvascular endothelial cells. Therefore, we further examined whether ibrutinib could enhance ACE protein expression in pulmonary microvascular endothelial cells. The results revealed a significant increase in ACE protein expression in pulmonary tissues of the ibrutinib group (Figures 4I and 4J). Furthermore, we evaluated the potential effects of ibrutinib on human cardiac myocytes and fibroblasts. However, no significant induction of apoptosis in human cardiac myocytes (Figures S4A and S4B) or fibrosis in human cardiac fibroblasts (Figures S4C and S4D) was observed upon treatment with ibrutinib. Taken together, these findings suggest that pulmonary microvascular endothelial cells play a crucial role in the promotion of AF by ibrutinib.

Inhibition of the PI3K-AKT pathway in human pulmonary microvascular endothelial cells is the potential mechanism of ibrutinib-induced upregulation of angiotensin-converting enzyme

To investigate the potential mechanism underlying the upregulation of ACE in HPMECs induced by ibrutinib, we performed RNA sequencing on HPMECs treated with or without ibrutinib. Through this analysis, we identified 1009 differentially expressed genes between the ibrutinib group and the control group (Figure 5A). Further analysis using the Kyoto Encyclopedia of Genes and Genomes (KEGG) pathway revealed that these differentially expressed genes were primarily enriched in the PI3K-AKT signaling pathway (Figure 5B). To validate the involvement of the PI3K-AKT pathway, we conducted western blot analyses to assess the expression levels of PI3K and AKT. The results demonstrated that in ibrutinib-treated HPMECs, the phosphorylation levels of PI3K and AKT were decreased, while the total protein levels remained unchanged (Figure 5C). More importantly, we examined the effect of the PI3K activator, 740Y-P, on the upregulation of ACE expression induced by ibrutinib. The results showed that 740Y-P significantly inhibited the ibrutinib-induced upregulation of ACE expression (Figure 5D), accompanied by an increase in the phosphorylation levels of PI3K and AKT (Figure 5E). Based on these findings, it can be inferred that the inhibition of the PI3K-AKT pathway in HPMECs may be the primary mechanism responsible for the upregulation of ACE induced by ibrutinib.

Perindopril attenuated ibrutinib-induced left atrial remodeling and atrial fibrillation promotion by inhibiting angiotensin-converting enzyme activation and C-terminal Src kinase-Src signaling pathway

To investigate the potential attenuation of ibrutinib-induced AF promotion through the inhibition of ACE activation, rats administered with ibrutinib were simultaneously treated with perindopril for a duration of 4 weeks. *In vivo* electrophysiological study results demonstrated that

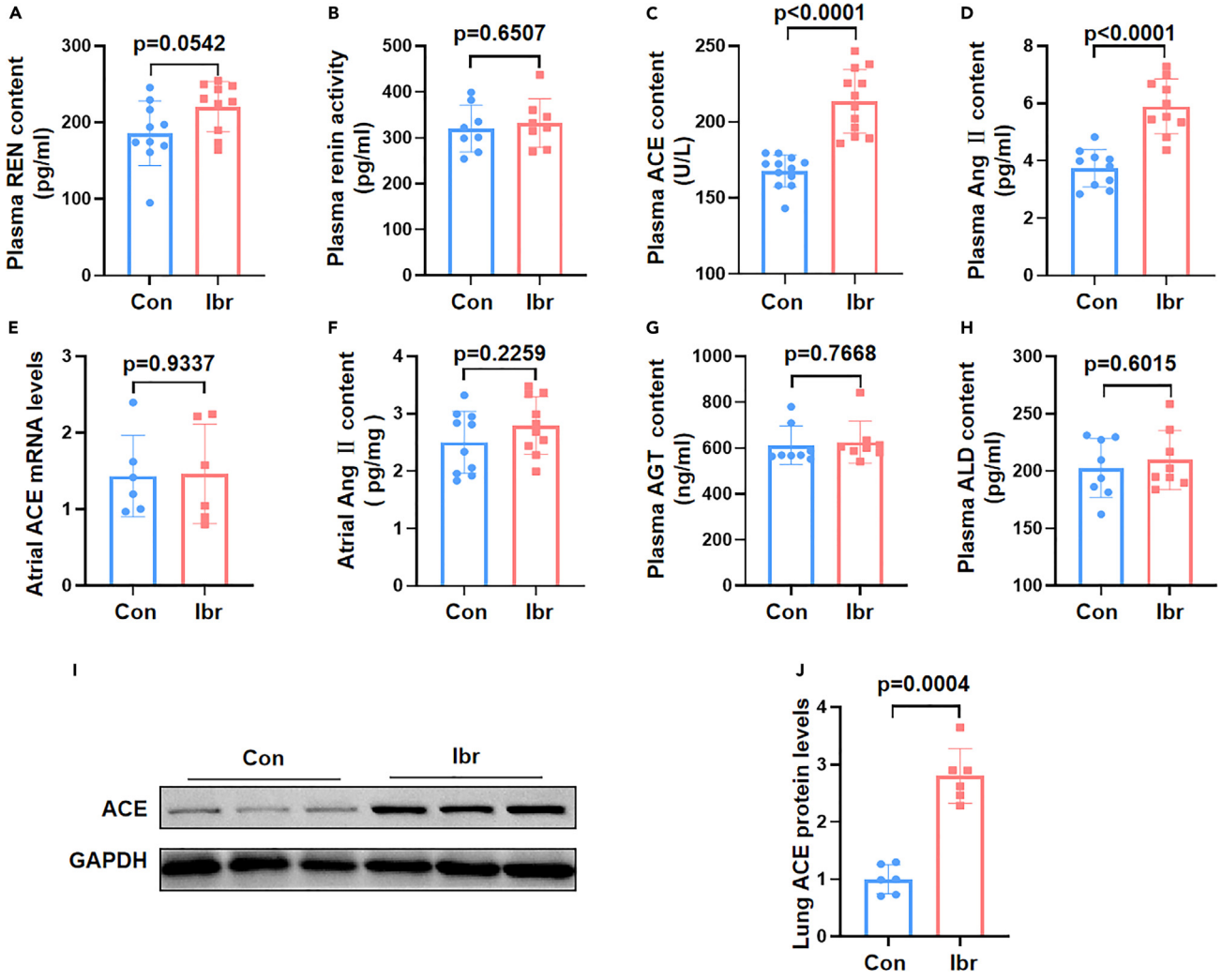

Figure 4. Ibrutinib elevates circulating ACE and Ang II levels

(A) Plasma REN content in the control and ibrutinib groups (n = 10 per group).

(B) Plasma renin activity content in the two groups (n = 8 per group).

(C) Plasma ACE content in the two groups (n = 12 per group).

(D) Plasma Ang II content in the two groups (n = 10 per group).

(E) Relative ACE mRNA levels in left atrial tissue of the two groups (n = 6 per group).

(F) Ang II content in left atrial tissue of the two groups (n = 10 per group).

(G) Plasma AGT content in the two groups (n = 8 per group).

(H) Plasma ALD content in the two groups (n = 8 per group).

(I and J) Representative Western blots and quantification of protein expressions of ACE in lung tissue of the two groups (n = 6 per group). Data are represented as mean ± SEM and compared by Student's *t* test. ACE = angiotensin converting enzyme; Ang II = Angiotensin II; renin = REN; angiotensinogen = AGT; aldosterone = ALD; Con = control group; Ibr = ibrutinib group.

perindopril significantly decreased AF inducibility (20% in the ibrutinib+perindopril group vs. 100% in the ibrutinib group; Figure 6A) and AF duration (1.61 ± 0.87 s in the ibrutinib+perindopril group vs. 32.87 ± 9.06 s in the ibrutinib group; Figure 6B) induced by ibrutinib (Figure S5A). Furthermore, perindopril treatment notably attenuated ibrutinib-induced left atrial enlargement (Figures 6C and S5B), left atrial fibrosis (Figures 6D and 6E), and left atrial downregulation of Cx40 and Cx40 (Figure 6F). We also measured pulmonary and plasma ACE levels, as well as plasma Ang II concentrations, in the control, ibrutinib, and ibrutinib+perindopril groups. The results demonstrated that perindopril treatment significantly inhibited the ibrutinib-induced increase in pulmonary and plasma ACE levels (Figures 7A and 7B) and plasma Ang II concentrations (Figure 7C). Regarding blood pressure, both systolic and diastolic readings showed decreases at the 3-week intervals in the perindopril group rats compared with the ibrutinib group rats, with no significant difference observed between the three groups at 1-, 2-, and 4-week intervals (Figure 7D). As expected, perindopril effectively mitigated the ibrutinib-induced downregulation of CSK and the

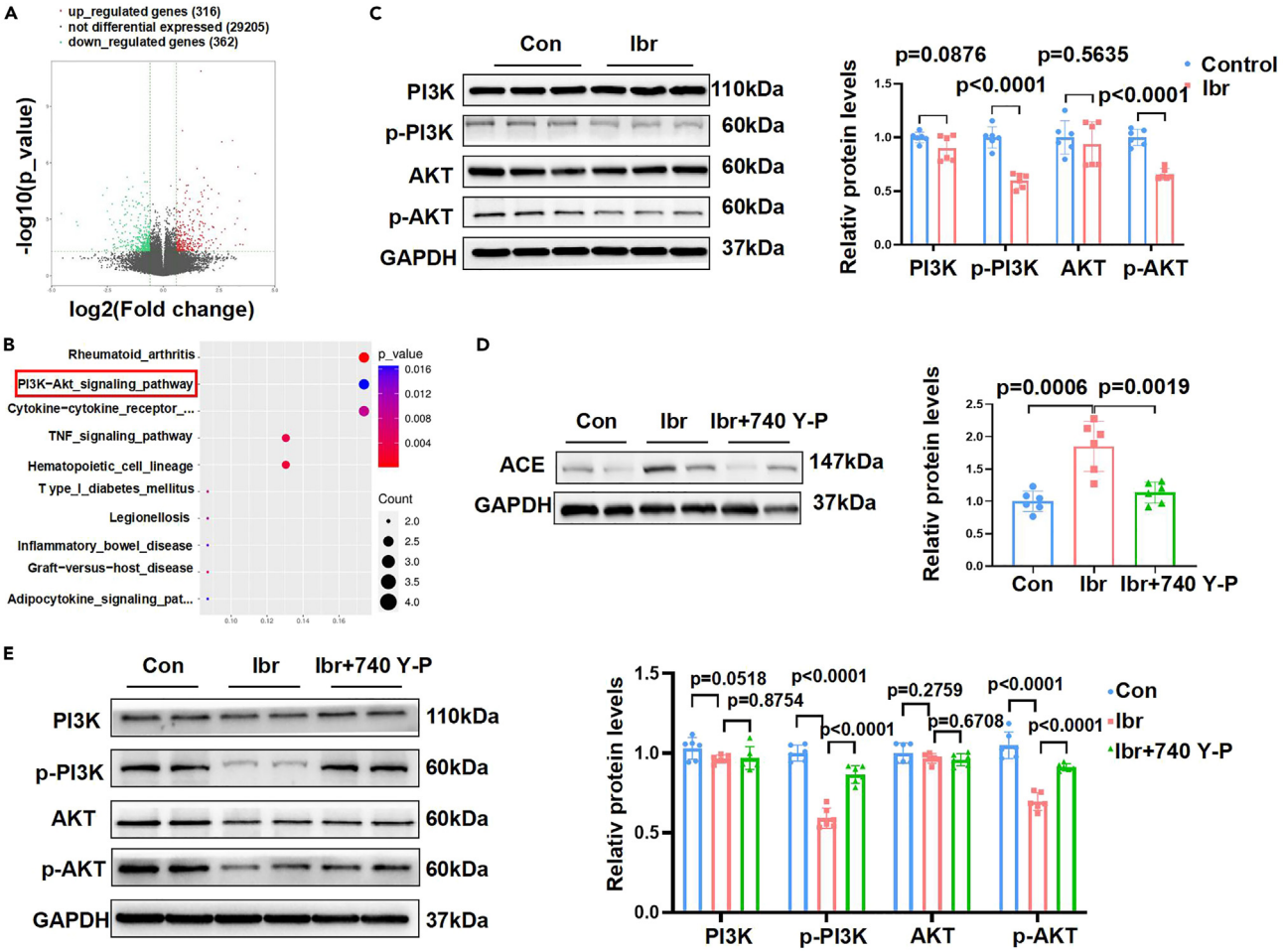

Figure 5. Inhibition of the PI3K-AKT pathway in pulmonary microvascular endothelial cells is the potential mechanism of ibrutinib-induced upregulation of ACE

(A) Volcano plot of differential expressed genes in HPMECs in the ibrutinib group relative to the control group, red represents up-regulated genes and blue represents down-regulated genes (n = 3 per group).

(B) The results of KEGG pathway analysis (n = 3 per group).

(C) Representative Western blots and quantification of protein expressions of PI3K, p-PI3K, AKT, and *p*-AKT in HPMECs of control and ibrutinib groups (n = 6 per group).

(D) Protein expressions of ACE in HPMECs of control, ibrutinib, and ibrutinib+740 Y-P groups (n = 6 per group).

(E) Protein expressions of PI3K, p-PI3K, AKT, and *p*-AKT in HPMECs of control, ibrutinib, and ibrutinib+740 Y-P groups (n = 6 per group). Data are represented as mean ± SEM and compared by Student's *t* test. p-PI3K = phosphorylated PI3K; *p*-AKT = phosphorylated AKT; ACE = angiotensin converting enzyme; Con = control group; Ibr = ibrutinib group.

phosphorylation of Src in left atrial tissues (Figure 7E). Additionally, perindopril attenuated the decrease in pulmonary phosphorylation levels of PI3K and AKT induced by ibrutinib, while the total protein levels remained unchanged (Figures S6A and S6B). In summary, our study demonstrates that perindopril effectively mitigates ibrutinib-induced left atrial remodeling and the promotion of atrial fibrillation through the inhibition of ACE activation and the CSK-Src signaling pathway, shedding light on potential therapeutic strategies to counteract the cardiovascular toxicities associated with ibrutinib treatment.

DISCUSSION

Our present study provides evidence that the oral administration of ibrutinib for a duration of 4 weeks in rats significantly increased vulnerability to AF. This increased susceptibility was accompanied by atrial fibrosis and downregulation of atrial Cx40 and Cx43. Importantly, our study is the first to demonstrate that ibrutinib acts as a potent inducer of Ang II by upregulating ACE expression in pulmonary microvascular endothelial cells through the inhibition of the PI3K-AKT signaling pathway. The elevated levels of circulating Ang II subsequently activate Src through the inhibition of CSK in the left atrial, leading to left atrial remodeling and the development of AF. Furthermore, our study provides

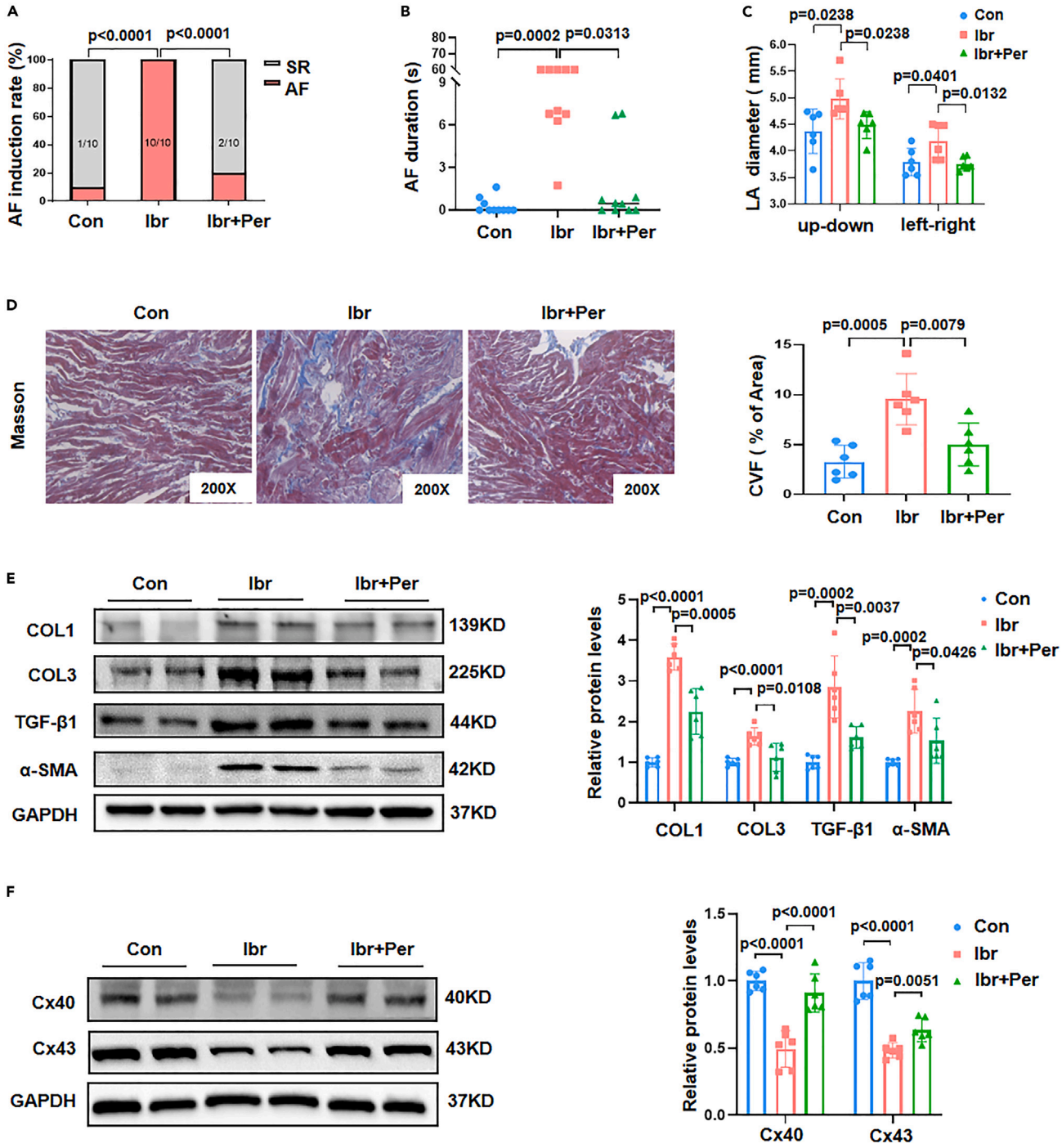

Figure 6. Perindopril attenuated ibrutinib-induced left atrial remodeling and AF promotion

(A) AF inducibility in the control, ibrutinib, and ibrutinib+perindopril groups (n = 10 per group).

(B) AF duration in the three groups (n = 10 per group).

(C) LA diameter in the three groups (n = 6 per group).

(D) Representative Masson's trichrome staining images and CVF of left atrial tissue (n = 6 per group).

(E) Protein expressions of Col I, Col III, α-SMA, and TGF-β1 in left atrial tissue (n = 6 per group).

(F) Left atrial CX40 and CX43 protein expressions (n = 6 per group). AF inducibility (A) was presented as numbers and compared by using the Fisher exact test. Data (B–F) are expressed as mean ± SEM and compared by Wilcoxon test (B) or Student's *t* test (C–F). AF = atrial fibrillation; SR = sinus rhythm; LA = left atrial; CVF = collagen volume fraction; Col I = collagen I; Col III = collagen III; Cx40 = connexin 40; Cx43 = connexin 43; Con = control group; Ibr = ibrutinib group; Ibr+Per = ibrutinib + perindopril group.

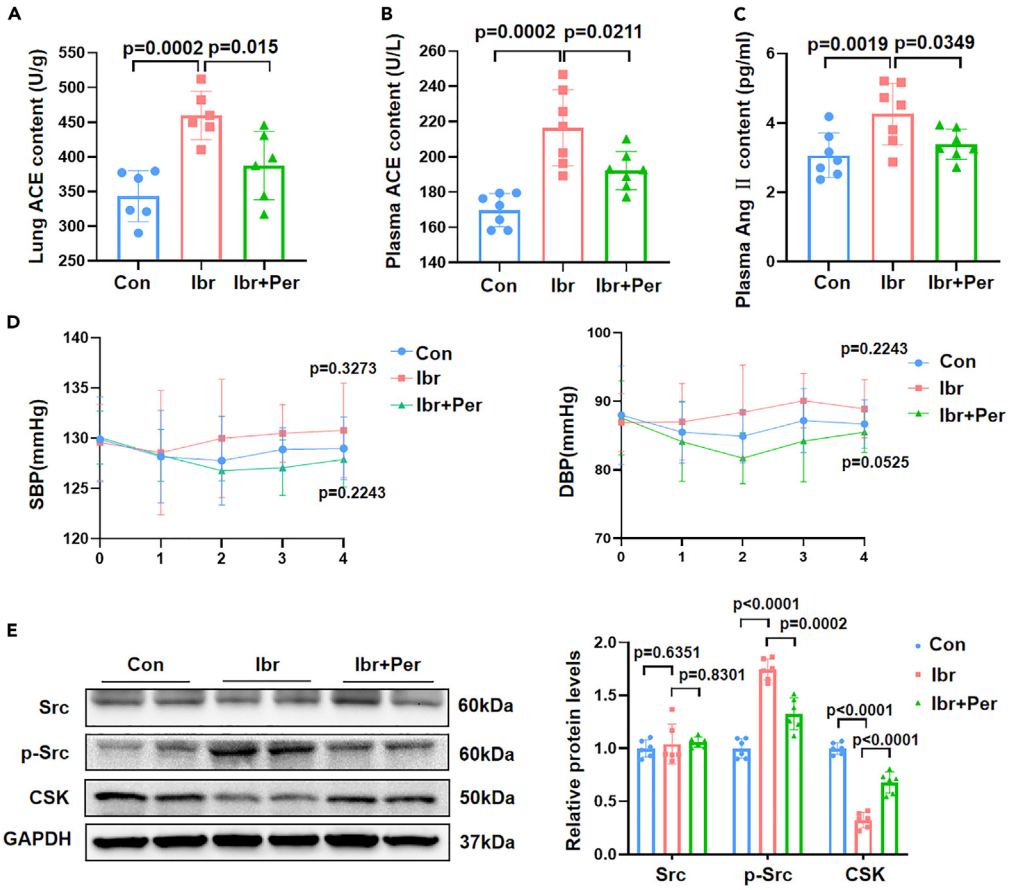

Figure 7. Perindopril inhibited ibrutinib-induced activation of ACE and CSK-Src signaling pathway

(A) Lung ACE content in the control, ibrutinib, and ibrutinib+perindopril groups (n = 6 per group).

(B) Plasma ACE content in the three groups (n = 6 per group).

(C) Plasma Ang II in the three groups (n = 6 per group).

(D) SBP and DBP in the three groups (n = 10 per group).

(E) Representative Western blots and quantification of protein expressions of Src, *p*-Src, and CSK in left atrial tissue of the three groups (n = 6 per group). Data are represented as mean ± SEM and compared by Tukey tests. ACE = angiotensin converting enzyme; Ang II = Angiotensin II; SBP = systolic blood pressure; DBP = diastolic blood pressure; *p*-Src = phosphorylated Src; Con = control group; Ibr = ibrutinib group; Ibr+Per = ibrutinib + perindopril group.

evidence that the ACE inhibitor perindopril effectively prevents ibrutinib-induced susceptibility left atrial remodeling and the promotion of AF by modulating the atrial CSK-Src signaling pathway.

Ibrutinib, as the first irreversible Bruton tyrosine kinase inhibitor, has proven to be an effective treatment for various B-cell lymphomas.[1] However, there is accumulating evidence indicating an increased incidence of AF in patients undergoing ibrutinib treatment.[2–4] A retrospective study revealed that new-onset AF in patients with cancer is associated with an elevated risk of thromboembolism and heart failure, even after adjusting for known risk factors.[6] Moreover, the management of ibrutinib-associated AF poses challenges due to its interactions with multiple medications commonly used for AF management,[3] and it also heightens the risk of bleeding, even without concurrent use of anticoagulants.[19,20] Therefore, understanding the underlying mechanisms of ibrutinib-induced AF may aid in identifying preventive measures.

Limited studies have investigated the arrhythmogenic mechanisms underlying ibrutinib-associated AF.[9–12] These studies have suggested that atrial structural remodeling is likely the underlying mechanism for ibrutinib-induced AF,[10–12] and the off-target inhibition of CSK by ibrutinib may be the main molecular pathway involved in this process.[12] CSK functions as a major endogenous inhibitor of Src family tyrosine kinases. Phosphorylation of the C-terminal domain by CSK inactivates Src, whereas the inhibition of CSK leads to Src activation. However, it remains unclear whether the ibrutinib's inhibition of CSK results in atrial Src activation. Previous study demonstrated that Ang II could induce the activation of CSK and thereby inhibiting Src activity in cultured rat aortic vascular smooth muscle cells.[21] In our present study, we have demonstrated for the first time that atrial Src is activated after 4 weeks of ibrutinib administration. Src activation has been shown to play a crucial role in Ang II-induced cardiac fibrosis and the reduction of cardiac Cx43. Inhibition of Src has been found to attenuate angiotensin II-mediated cardiac fibrosis and dysregulation of Cx43.[17,18,22] Atrial fibrosis is a characteristic feature of arrhythmogenic structural remodeling and is known to play a significant role in initiating and sustaining AF.[15,23,24] Moreover, downregulation of Cx43 contributes to slowed atrial

conduction and enhanced atrial fibrotic response. Studies have demonstrated that the overexpression of Cx43 successfully inhibits AF progression in a porcine model, as reviewed by Nattel et al.[25] Therefore, our findings provide a possible mechanistic link between ibrutinib-induced CSK inhibition and left atrial remodeling, as previously described by Xiao et al.[12]

Previous studies have reported that Src family protein kinases in cardiac fibroblasts, cardiomyocytes, and smooth muscle cells are primarily activated by Ang II.[14] Therefore, we determined whether ibrutinib could induce ACE activation and increase Ang II levels. Interestingly and surprisingly, we found that ibrutinib significantly induced ACE expression in pulmonary tissues *in vivo* and in HPMECs *in vitro*, thereby leading to increased circulating Ang II levels. In addition, our study indicated the inhibition of the PI3K-AKT pathway in pulmonary microvascular endothelial cells might be the main molecular mechanism of ibrutinib-induced ACE upregulation. Consistent with our findings, a previous study reported that ibrutinib significantly reduced PI3K-Akt activity in neonatal rat ventricular myocytes.[9] To the best of our knowledge, this is the first study to demonstrate the activating effect of ibrutinib on the ACE. Activation of the RAS has been well-documented to contribute to cardiac arrhythmia, hypertension, cardiovascular remodeling, and heart failure by regulating various signal transduction cascades.[14] Moreover, a recent study revealed a significant increase in the incidence of ventricular arrhythmia, hypertension, and heart failure in patients treated with ibrutinib, in addition to atrial fibrillation.[2] Therefore, our findings provide a potential explanation for the observed cardiovascular toxicities associated with ibrutinib, although no differences in blood pressure and left ventricular function were found in this short-term rat model.

Accumulating evidence highlights the significant role of the RAS in the etiopathogenesis of AF.[15] Clinical trials have demonstrated the effectiveness of RAS inhibitors in the primary and secondary prevention of AF.[16,26,27] Importantly, experimental studies have also shown that ACE inhibitors and Ang II receptor blockers can protect against chemotherapy-induced cardiotoxicity.[28,29] Recent systematic reviews and meta-analyses of clinical randomized controlled trials have indicated that RAS inhibitors have a substantial protective effect on the reduction of left ventricular ejection fraction induced by chemotherapeutic drugs.[30,31] In our present study, we provide the first description of the effective prevention of ibrutinib-induced left atrial remodeling and AF promotion by the ACE inhibitor perindopril. This effect was accompanied by the attenuation of CSK downregulation and Src activation, suggesting that the modulation of the CSK-Src signaling pathway contributes to the observed benefits. Further clinical studies are warranted to confirm these preliminary findings in our animal model. Interestingly, a growing number of preclinical observations have highlighted the importance of the RAS in cancer development, growth, and progression.[32] The use of ACE inhibitors or Ang II receptor blockers has been significantly associated with improved cancer progression-free and overall survival.[32,33] Our findings suggest that Ibrutinib may modulate components of the RAS, such as ACE and Ang II, and further research is warranted to explore the potential implications of this modulation in the context of atrial fibrillation. Understanding the precise mechanisms by which Ibrutinib affects RAS components in the atria can offer insights into its role in the development of atrial fibrillation and guide the exploration of novel prevention strategies.

In conclusion, our study demonstrates that ibrutinib induces ACE expression in pulmonary microvascular endothelial cells through the inhibition of the PI3K-AKT pathway. This leads to an increase in circulating levels of Ang II and subsequent promotion of left atrial remodeling through the downstream regulation of CSK-Src signaling, ultimately culminating in AF. Importantly, our findings highlight the efficacy of ACE inhibitor perindopril in preventing ibrutinib-induced AF by modulating these associated pathways.

Limitation of the study

As is well known, Ang II exerts its physiological functions through two distinct receptor subtypes: the type 1 receptor and type 2 receptor. However, the specific receptor subtype mediating the effects of Ang II was not clarified in the present experiment.

STAR★METHODS

Detailed methods are provided in the online version of this paper and include the following:

- KEY RESOURCES TABLE
- RESOURCE AVAILABILITY
  - Lead contact
  - Materials availability
  - Data and code availability
- EXPERIMENTAL MODEL AND SUBJECT DETAILS
  - Experimental animals
  - Cell culture
- METHOD DETAILS
  - Blood pressure measurement
  - In vivo electrophysiological study
  - Echocardiography
  - HE and Masson's trichrome staining
  - Enzyme-Linked Immunosorbent Assay
  - Western blot analysis
  - RNA extraction and quantitative real-time qRT-PCR
  - Immunofluorescence staining

- TUNEL staining
- Transcriptome sequencing

- QUANTIFICATION AND STATISTICAL ANALYSIS

SUPPLEMENTAL INFORMATION

Supplemental information can be found online at https://doi.org/10.1016/j.isci.2024.108926.

ACKNOWLEDGMENTS

This work was supported by grants from the HMU Marshal Initiative Funding (HMUMIF-22001, China) and the Supporting Project for Outstanding Young Medical Talents of the First Affiliated Hospital of Harbin Medical University (No. HYD2020JQ0001). This work was also supported by grants from the National Natural Science Foundation of China (No. 82070336) and the State Key Program of the National Natural Science Foundation of China (No.81830012).

AUTHOR CONTRIBUTIONS

Y.G. and S.Y. designed the research. S.Y., L.L., H.H., Q.L., Z.W., and Y.D. performed *in vivo* experiments. W.X., N.Y., X.Z., Y.Z., and S.Z. performed *in vitro* experiments. N.F. and S.Y. analyzed data. Y.L. provided guidance on experimental designs. S.Y. wrote the article with input from all authors.

DECLARATION OF INTERESTS

The authors declare that they have no competing interests.

Received: August 8, 2023
Revised: October 25, 2023
Accepted: January 12, 2024
Published: January 17, 2024

REFERENCES

1. Pal-Singh, S., Dammeijer, F., and Hendriks, R.W. (2018). Role of Bruton's tyrosine kinase in B cells and malignancies. Mol. Cancer *17*, 57.
2. Salem, J.E., Manouchehri, A., Bretagne, M., Lebrun-Vignes, B., Groarke, J.D., Johnson, D.B., Yang, T., Reddy, N.M., Funck-Brentano, C., Brown, J.R., et al. (2019). Cardiovascular Toxicities Associated With Ibrutinib. J. Am. Coll. Cardiol. *74*, 1667–1678.
3. Ganatra, S., Sharma, A., Shah, S., Chaudhry, G.M., Martin, D.T., Neilan, T.G., Mahmood, S.S., Barac, A., Groarke, J.D., Hayek, S.S., et al. (2018). Ibrutinib-Associated Atrial Fibrillation. JACC Clin. Electrophysiol. *4*, 1491–1500.
4. Archibald, W.J., Rabe, K.G., Kabat, B.F., Herrmann, J., Ding, W., Kay, N.E., Kenderian, S.S., Muchtar, E., Leis, J.F., Wang, Y., et al. (2021). Atrial fibrillation in patients with chronic lymphocytic leukemia (CLL) treated with ibrutinib: risk prediction, management, and clinical outcomes. Ann. Hematol. *100*, 143–155.
5. Mato, A.R., Hill, B.T., Lamanna, N., Barr, P.M., Ujjani, C.S., Brander, D.M., Howlett, C., Skarbnik, A.P., Cheson, B.D., Zent, C.S., et al. (2017). Optimal sequencing of ibrutinib, idelalisib, and venetoclax in chronic lymphocytic leukemia: results from a multicenter study of 683 patients. Ann. Oncol. *28*, 1050–1056.
6. Hu, Y.F., Liu, C.J., Chang, P.M., Tsao, H.M., Lin, Y.J., Chang, S.L., Lo, L.W., Tuan, T.C., Li, C.H., Chao, T.F., et al. (2013). Incident thromboembolism and heart failure associated with new-onset atrial fibrillation in cancer patients. Int. J. Cardiol. *165*, 355–357.
7. Caron, F., Leong, D.P., Hillis, C., Fraser, G., and Siegal, D. (2017). Current understanding of bleeding with ibrutinib use: a systematic review and meta-analysis. Blood Adv. *1*, 772–778.
8. Brown, J.R., Moslehi, J., Ewer, M.S., O'Brien, S.M., Ghia, P., Cymbalista, F., Shanafelt, T.D., Fraser, G., Rule, S., Coutre, S.E., et al. (2019). Incidence of and risk factors for major haemorrhage in patients treated with ibrutinib: An integrated analysis. Br. J. Haematol. *184*, 558–569.
9. McMullen, J.R., Boey, E.J., Ooi, J.Y., Seymour, J.F., Keating, M.J., and Tam, C.S. (2014). Ibrutinib increases the risk of atrial fibrillation, potentially through inhibition of cardiac PI3K-Akt signaling. Blood *124*, 3829–3830.
10. Jiang, L., Li, L., Ruan, Y., Zuo, S., Wu, X., Zhao, Q., Xing, Y., Zhao, X., Xia, S., Bai, R., et al. (2019). Ibrutinib promotes atrial fibrillation by inducing structural remodeling and calcium dysregulation in the atrium. Heart Rhythm *16*, 1374–1382.
11. Yang, X., An, N., Zhong, C., Guan, M., Jiang, Y., Li, X., Zhang, H., Wang, L., Ruan, Y., Gao, Y., et al. (2020). Enhanced cardiomyocyte reactive oxygen species signaling promotes ibrutinib-induced atrial fibrillation. Redox Biol. *30*, 101432.
12. Xiao, L., Salem, J.E., Clauss, S., Hanley, A., Bapat, A., Hulsmans, M., Iwamoto, Y., Wojtkiewicz, G., Cetinbas, M., Schloss, M.J., et al. (2020). Ibrutinib-Mediated Atrial Fibrillation Attributable to Inhibition of C-Terminal Src Kinase. Circulation *142*, 2443–2455.
13. Okada, M. (2012). Regulation of the SRC family kinases by Csk. Int. J. Biol. Sci. *8*, 1385–1397.
14. Forrester, S.J., Booz, G.W., Sigmund, C.D., Coffman, T.M., Kawai, T., Rizzo, V., Scalia, R., and Eguchi, S. (2018). Angiotensin II Signal Transduction: An Update on Mechanisms of Physiology and Pathophysiology. Physiol. Rev. *98*, 1627–1738.
15. Chen, Y.C., Voskoboinik, A., Gerche, A., Marwick, T.H., and McMullen, J.R. (2021). Prevention of Pathological Atrial Remodeling and Atrial Fibrillation: JACC State-of-the-Art Review. J. Am. Coll. Cardiol. *77*, 2846–2864.
16. Khatib, R., Joseph, P., Briel, M., Yusuf, S., and Healey, J. (2013). Blockade of the renin-angiotensin-aldosterone system (RAAS) for primary prevention of non-valvular atrial fibrillation: a systematic review and meta analysis of randomized controlled trials. Int. J. Cardiol. *165*, 17–24.
17. Tao, X., Fan, J., Kao, G., Zhang, X., Su, L., Yin, Y., and Zrenner, B. (2014). Angiotensin-(1-7) attenuates angiotensin II-induced signalling associated with activation of a tyrosine phosphatase in Sprague-Dawley rats cardiac fibroblasts. Biol. Cell. *106*, 182–192.
18. Sovari, A.A., Iravanian, S., Dolmatova, E., Jiao, Z., Liu, H., Zandieh, S., Kumar, V., Wang, K., Bernstein, K.E., Bonini, M.G., et al. (2011). Inhibition of c-Src tyrosine kinase prevents angiotensin II-mediated connexin-43 remodeling and sudden cardiac death. J. Am. Coll. Cardiol. *58*, 2332–2339.
19. Bye, A.P., Unsworth, A.J., Vaiyapuri, S., Stainer, A.R., Fry, M.J., and Gibbins, J.M. (2015). Ibrutinib Inhibits Platelet Integrin αIIbβ3 Outside-In Signaling and Thrombus

Stability But Not Adhesion to Collagen. Arterioscler. Thromb. Vasc. Biol. *35*, 2326–2335.

20. Lee, R.H., Piatt, R., Conley, P.B., and Bergmeier, W. (2017). Effects of ibrutinib treatment on murine platelet function during inflammation and in primary hemostasis. Haematologica *102*, e89–e92.
21. Liu, J., Shimosawa, T., Matsui, H., Meng, F., Supowit, S.C., DiPette, D.J., Ando, K., and Fujita, T. (2007). Adrenomedullin inhibits angiotensin II-induced oxidative stress via Csk-mediated inhibition of Src activity. Am. J. Physiol. Heart Circ. Physiol. *292*, H1714–H1721.
22. Lu, L., Cao, L., Liu, Y., Chen, Y., Fan, J., and Yin, Y. (2021). Angiotensin (ang) 1-7 inhibits ang II-induced atrial fibrosis through regulating the interaction of proto-oncogene tyrosine-protein kinase Src (c-Src) and Src homology region 2 domain-containing phosphatase-1 (SHP-1)). Bioengineered *12*, 10823–10836.
23. Delgado, V., Di-Biase, L., Leung, M., Romero, J., Tops, L.F., Casadei, B., Marrouche, N., and Bax, J.J. (2017). Structure and Function of the Left Atrium and Left Atrial Appendage: AF and Stroke Implications. J. Am. Coll. Cardiol. *70*, 3157–3172.
24. Hongting, H., Sen, Y., Xinbo, Z., Han, X., Fang, N., Zhang, Y., Dai, C., Li, W., Yu, H., Gao, Y., et al. (2022). Atrial myocyte-derived exosomal microRNA contributes to atrial fibrosis in atrial fibrillation. J. Transl. Med. *20*, 407.
25. Nattel, S., Heijman, J., Zhou, L., and Dobrev, D. (2020). Molecular Basis of Atrial Fibrillation Pathophysiology and Therapy: A Translational Perspective. Circ. Res. *127*, 51–72.
26. Marott, S.C., Nielsen, S.F., Benn, M., and Nordestgaard, B.G. (2014). Antihypertensive treatment and risk of atrial fibrillation: a nationwide study. Eur. Heart J. *35*, 1205–1214.
27. Peng, L., Li, Z., Luo, Y., Tang, X., Shui, X., Xie, X., Zheng, Z., Dong, R., Liu, J., Zhu, J., and Li, S. (2020). Renin-Angiotensin System Inhibitors for the Prevention of Atrial Fibrillation Recurrence After Ablation - A Meta-Analysis. Circ. J. *84*, 1709–1717.
28. Hullin, R., Métrich, M., Sarre, A., Basquin, D., Maillard, M., Regamey, J., and Martin, D. (2018). Diverging effects of enalapril or eplerenone in primary prevention against doxorubicin-induced cardiotoxicity. Cardiovasc. Res. *114*, 272–281.
29. Mozolevska, V., Schwartz, A., Cheung, D., Goyal, V., Shaikh, B., Dingman, B., Kim, E., Mittal, I., Asselin, C.Y., Edel, A., et al. (2019). Role of renin-angiotensin system antagonists in the prevention of bevacizumab- and sunitinib-mediated cardiac dysfunction. Am. J. Physiol. Heart Circ. Physiol. *316*, H446–H458.
30. Li, X., Li, Y., Zhang, T., Xiong, X., Liu, N., Pang, B., Ruan, Y., Gao, Y., Shang, H., and Xing, Y. (2020). Role of cardioprotective agents on chemotherapy-induced heart failure: A systematic review and network meta-analysis of randomized controlled trials. Pharmacol. Res. *151*, 104577.
31. Lewinter, C., Nielsen, T.H., Edfors, L.R., Linde, C., Bland, J.M., LeWinter, M., Cleland, J.G.F., Køber, L., Braunschweig, F., and Mansson-Broberg, A. (2022). A systematic review and meta-analysis of beta-blockers and renin-angiotensin system inhibitors for preventing left ventricular dysfunction due to anthracyclines or trastuzumab in patients with breast cancer. Eur. Heart J. *43*, 2562–2569.
32. Pinter, M., and Jain, R.K. (2017). Targeting the renin-angiotensin system to improve cancer treatment: Implications for immunotherapy. Sci. Transl. Med. *9*, 410.
33. Perini, M.V., Dmello, R.S., Nero, T.L., and Chand, A.L. (2020). Evaluating the benefits of renin-angiotensin system inhibitors as cancer treatments. Pharmacol. Ther. *211*, 107527.
34. Zhu, Z., Li, H., Chen, W., Cui, Y., Huang, A., and Qi, X. (2020). Perindopril Improves Cardiac Function by Enhancing the Expression of SIRT3 and PGC-1α in a Rat Model of Isoproterenol-Induced Cardiomyopathy. Front. Pharmacol. *11*, 94.
35. Zhang, Y., Sun, D., Zhao, X., Luo, Y., Yu, H., Zhou, Y., Gao, Y., Han, X., Duan, Y., Fang, N., et al. (2022). Bacteroides fragilis prevents aging-related atrial fibrillation in rats via regulatory T cells-mediated regulation of inflammation. Pharmacol. Res. *177*, 106141.
36. Dai, H., Wang, X., Yin, S., Zhang, Y., Han, Y., Yang, N., Xu, J., Sun, L., Yuan, Y., Sheng, L., et al. (2017). Atrial Fibrillation Promotion in a Rat Model of Rheumatoid Arthritis. J. Am. Heart Assoc. *6*.

STAR★METHODS

KEY RESOURCES TABLE

REAGENT or RESOURCE	SOURCE	IDENTIFIER
Antibodies		
Rabbit monoclonal anti-Collagen I	Abcam	Ca#ab260043;RRID_AB_2922767
Rabbit monoclonal anti-Collagen III	Abcam	Ca#ab7778;RRID_AB_306066
Rabbit monoclonal anti-α-SMA	Abcam	Ca#ab5694;RRID_AB_2223021
Rabbit monoclonal anti-TGF-β1	Abcam	Ca#ab215715;RRID_AB_2893156
Rabbit monoclonal anti-ACE	Abcam	Ca#ab254222;RRID_AB_3073965
Rabbit monoclonal anti-CSK(C74C1)	Cell Signaling Technology	Ca#4980;RRID_AB_2276592
Rabbit monoclonal anti-Src	Cell Signaling Technology	Ca#2108;RRID_AB_331137
Rabbit monoclonal anti-phosphp-Src(Tyr416)	Cell Signaling Technology	Ca#2101;RRID_AB_331697
Rabbit polyclonal anti-CX40	Biosynthesis Biotechnology	Ca#bs-1050R;RRID_AB_10857532
Rabbit polyclonal anti-CX43	Cell Signaling Technology	Ca#3512;RRID_AB_2294590
Rabbit polyclonal anti-PI3 Kinase p110 alpha	Cell Signaling Technology	Ca#4255;RRID_AB_659888
Rabbit polyclonal anti-phospho-PI3 Kinase p85 (Tyr458)/p55 (Tyr199)	Cell Signaling Technology	Ca#4228S;RRID_AB_659940
Rabbit polyclonal anti-AKT	Cell Signaling Technology	Ca#9272;RRID_AB_329827
Rabbit monoclonal anti-phospho-AKT(Ser473)	Cell Signaling Technology	Ca#4060;RRID_AB_2315049
Chemicals, peptides, and recombinant proteins		
Ibrutinib	Catalent CTS	Cat#:1946974;CAS:936563-96-1
perindopril	Servier Pharmaceutical	Cat#:070307;CAS:82834-16-0
Dimethylsulfoxide	Sigma-Aldrich	Cat#:D8370;CAS:67-68-5
Ibrutinib	Selleckchem	Cat#:S2680;CAS:936563-96-1
740Y-P	MedChemExpress	Cat#:HY-P0175;CAS:1236188-16-1
Experimental models: Cell lines		
HPMECs	Pricells Biopharma	HUM-CELL-0001
Human cardiomyocytes (AC16 cells)	Bena Culture Collection	BNCC 339980
Human heart fibroblasts	Bena Culture Collection	BNCC 354381
Experimental models: Organisms/strains		
SD rat	Beijing Vital River Laboratory Animal Technology Co, Ltd (Beijing, China)	NA
Oligonucleotides		
qRT-PCR primers	See Table S1	NA

RESOURCE AVAILABILITY

Lead contact

Further information and requests for resources and reagents should be directed to and will be fulfilled by the lead contact, Yue Li (ly99ly@vip.163.com).

Materials availability

This study did not generate new unique reagents.

Data and code availability

RNA-seq data generated for this article have been deposited at NCBI's Sequence Read Archive (SRA) and are publicly available as of the date of publication. The project number is PRJNA1052465.

This paper does not report original code.

Any additional information required to reanalyze the data reported in this paper is available from the lead contact upon request.

EXPERIMENTAL MODEL AND SUBJECT DETAILS

Experimental animals

All animal procedures in this study were conducted in accordance with the Health Guide for the Care and Use of Laboratory Animals and approved by the Animal Care Committee at Harbin Medical University (IACUC number: 2021121) to ensure humane care. Seventy male SD rats weighing 260-280g with a mean age of 8 weeks were obtained from Beijing Vital River Laboratory Animal Technology Co, Ltd (Beijing, China) and housed at the Experimental Animal Center of Harbin Medical University. The rats were randomly assigned and individually housed in a 12:12 h light-dark cycle, with *ad libitum* access to food and water. For the experimental groups, rats in the ibrutinib group were orally administered ibrutinib (17 mg/kg/d; Catalent CTS, LLC, USA) for a duration of 4 weeks. The dosage of ibrutinib was determined based on body surface area, as previously described.[10] Rats in the ibrutinib + perindopril group received both ibrutinib and perindopril (2 mg/kg/d[34]) orally for 4 weeks. Control rats received the vehicle solution in parallel. The vehicle solution was prepared using dimethylsulfoxide (DMSO; Sigma-Aldrich, Natick, MA, USA) as a solvent for dissolving ibrutinib.

Cell culture

HPMECs were obtained from Pricells Biopharma Ltd. (Wuhan, China). Human cardiomyocytes (AC16 cells) were sourced from the Bena Culture Collection (BNCC 339980, China), and human heart fibroblasts were also obtained from the Bena Culture Collection (BNCC 354381, China). Ibrutinib, a Bruton tyrosine kinase inhibitor, was purchased from Selleckchem (Houston, TX, USA), while the PI3K activator 740Y-P was obtained from MedChemExpress (Princeton, NJ, USA). HPMECs were cultured in RPMI-1640 medium (HyClone; GE Healthcare Life Sciences, Logan, UT, USA) supplemented with 10% fetal bovine serum (FBS; Gibco, USA) and 1% penicillin/streptomycin (P/S; Gibco, USA). Human cardiomyocytes and human heart fibroblasts were cultured in Dulbecco's Modified Eagle Medium (DMEM; Gibco, USA), enriched with 10% fetal bovine serum (FBS; Gibco, USA) and 1% penicillin/streptomycin (P/S; Gibco, USA). The cells were maintained in a humidified incubator at 37°C with 5% CO2. For the experimental treatments, HPMECs were incubated with different solutions: DMSO only (control group), DMSO supplemented with 0.3 μM ibrutinib[9] (ibrutinib group), and DMSO supplemented with 0.3 μM ibrutinib and 50 μM 740Y-P (ibrutinib + 740Y-P group). Similarly, human cardiomyocytes and human heart fibroblasts were subjected to different treatments: DMSO only (control group), DMSO supplemented with 0.3 μM ibrutinib[9] (ibrutinib group). The incubation period lasted for 48 hours, allowing sufficient time for the effects of the compounds to manifest.

METHOD DETAILS

Blood pressure measurement

Blood pressure measurements were performed at baseline and weekly throughout the 4-week study using a tail-cuff system (Softron BP-2010; Softron Tokyo, Japan) on conscious rats.

In vivo electrophysiological study

AF induction followed the same protocol as previously described in detail.[35] Briefly, rats were anesthetized with 1% sodium pentobarbital (30 mg/kg) administered via peritoneal injection. Open-chest surgery was performed, and a 1.9-F octapolar catheter (Transonic Systems Inc., New York, USA) was positioned on the right atrium for programmed stimulus delivery. AF inducibility was assessed using 50-Hz burst pacing, consisting of 12 bursts separated by a 2-second interval, applied for 3 seconds. AF was defined as the presence of irregular atrial electrograms (>800 beats/min) with an irregular ventricular response lasting for more than 1 second. AF duration was determined as the average duration of all AF episodes within a 60-second period for each rat.

Echocardiography

Transthoracic echocardiographic studies were conducted using the Philips CX50 ultrasound system equipped with a Philips S12-4 phased-sector ultrasound transducer while rats were under sedation. We obtained measurements of the following parameters using established protocols: Left atrial (LA) diameter at end-diastole, Interventricular septum diastolic (IVSD), Interventricular septum systolic (IVSS), Left ventricular internal dimension diastole (LVIDD), Left ventricular internal dimension systole (LVIDS), Left ventricular posterior wall in diastole (LVPWD), Left ventricular posterior wall in systole (LVPWS).[36]

HE and Masson's trichrome staining

Left atrial tissues were subjected to histological staining using HE and Masson's trichrome techniques. HE staining allowed for the visualization of cellular components and tissue morphology. Masson's trichrome staining was employed to assess collagen deposition and fibrosis in the left atrial tissues. To quantify the extent of collagen deposition, the collagen volume fraction was determined by calculating the ratio of the area occupied by collagen fibers to the total area in the visual field. This analysis was performed using Image-Pro Plus software, enabling accurate and standardized measurements.

Enzyme-Linked Immunosorbent Assay

The concentrations of plasma ACE and Ang II, as well as the Ang II content in atrial tissues, were assessed using ELISA kits (BlueGene Biotech Co Ltd, Shanghai, China). Meanwhile, the concentrations of plasma renin (REN), angiotensinogen (AGT), and aldosterone (ALD) were determined employing ELISA kits (Elabscience Biotechnology Co Ltd, Wuhan, China). Specifically, the concentrations of renin activity were measured using ELISA kits from Jianglai Biotechnology Co Ltd, Shanghai, China. All measurements were conducted in accordance with the manufacturer's instructions supplied with the respective kits.

Western blot analysis

Protein samples were subjected to 10% SDS-polyacrylamide gel electrophoresis to separate the proteins, followed by their transfer onto polyvinylidene difluoride membranes. The membranes were then incubated in 5% nonfat milk at room temperature for 90 minutes to block nonspecific binding. Subsequently, the membranes were incubated overnight at 4°C with primary antibodies. Antibodies against collagen I, collagen III, α-SMA, TGF-β1, and ACE were obtained from Abcam Biotechnology Company (Cambridge, UK), while antibodies against CSK, Src, p-Src (Tyr-416), Cx40, Cx43, PI3K, p-PI3K, AKT, and p-AKT were obtained from Cell Signaling Technology Inc. (Danvers, MA, USA). Following primary antibody incubation, the membranes were washed with PBST and then probed with secondary antibodies, either goat anti-rabbit or goat anti-mouse IgG HRP, for 1 hour at room temperature. After washing three times with PBST, the protein bands were visualized using an enhanced chemiluminescence detection system. The bound complexes were imaged using the Bio-Rad ChemiDoc TMXRS, and ImageJ software was utilized for gel image analysis.

RNA extraction and quantitative real-time qRT-PCR

Total RNA was extracted using a reagent from Axygen (USA). Real-time quantitative reverse transcription polymerase chain reaction (qRT-PCR) was carried out using an Applied Biosystems instrument. The specific primers used for amplifying ACE were as follows: forward primer, 5′-CACCGGCAAGGTCTGCTT-3′, and reverse primer, 5′-CTTGGCATAGTTTCGTGAGGAA-3′. The relative quantification of gene expression was determined using the 2^-ΔΔCT method, with normalization against GAPDH as an internal control.

Immunofluorescence staining

Cardiac fibroblasts were initially fixed with 4% paraformaldehyde for 20 minutes at room temperature. Subsequently, they were permeabilized using a 0.5% Triton X-100 solution for another 20 minutes at room temperature. For the immunofluorescence staining, the primary antibodies, including alpha-smooth muscle actin (α-SMA) antibody (1:100, Abcam, US), were incubated with the cells overnight at 4°C. Following this, the cells were treated with secondary antibodies (Beyotime, China, 1:200) for 90 minutes at room temperature. To visualize the nuclei, DAPI (Beyotime, China) was used for counterstaining. The stained cells were then examined using a laser scanning confocal microscope (ZEISS 510S, Germany).

TUNEL staining

TUNEL staining was performed following the manufacturer's instructions (Roche, Sigma, USA). In brief, cardiac myocytes were fixed with 4% paraformaldehyde for 20 minutes at room temperature. Subsequently, the cells were permeabilized using a 0.1% Triton X-100 solution for 20 minutes at room temperature. The TUNEL staining solution, a mixture of TdT enzyme and labeled dUTP, was prepared according to the kit instructions. Cells were then incubated at 37°C for 1 hour to facilitate labeling. Finally, cell nuclei were counterstained with a fluorescent nuclear marker such as DAPI for 10 minutes at room temperature. Cells were observed using a laser scanning confocal microscope (ZEISS 510S, Germany).

Transcriptome sequencing

The RNA level changes in HPMECs were analyzed using transcriptome sequencing (Sangon Biotech, China) with three biological replicates in each group.

QUANTIFICATION AND STATISTICAL ANALYSIS

Statistical analyses were conducted using GraphPad Prism 9.0 software (GraphPad Software, Inc, La Jolla, CA). The Shapiro-Wilk test was used to assess normality. Continuous variables were presented as mean ± standard error of the mean (SEM). Two-group comparisons were performed using Student's unpaired t-test or Wilcoxon (Mann–Whitney U) test. Variables with more than two groups were analyzed by one-way ANOVA followed by Tukey's tests for post hoc comparisons. Categorical variables were reported as numbers and percentages and compared using the Fisher's exact test. Statistical significance was defined as $P < 0.05$.